Published in Marine Geology 237, issues 1-2, 25-36, 2007
which should be used for any reference to this work

Late Holocene fine-grained sediments of the Balearic Abyssal Plain, Western Mediterranean Sea

D. Zúñiga [a], J. García-Orellana [b], A. Calafat [a,*], N.B. Price [c], T. Adatte [d], A. Sanchez-Vidal [a], M. Canals [a], J.A. Sanchez-Cabeza [e], P. Masqué [b], J. Fabres [a]

[a] *GRC Geociències Marines, Dept. d'Estratigrafia, Paleontologia i Geociències Marines, Universitat de Barcelona, E-08028, Barcelona, Spain*
[b] *Department de Física — Institut de Ciençia i Technologia Ambientals, Universitat Autònoma de Barcelona, E-08193, Bellaterra, Spain*
[c] *Department of Geology and Geophysics, University of Edinburgh, EH 9 3JW, Edinburgh, United Kingdom*
[d] *Institut de Géologie, Université de Neuchâtel, CH-2007, Neuchâtel, Switzerland*
[e] *Marine Environment Laboratory, International Atomic Energy Agency, MC-98000, Monaco*

Abstract

The Late Holocene fine-grained sedimentation in the deep central Balearic Abyssal Plain, Western Mediterranean Sea, has been studied after the analysis of high quality sediment cores from three multicoring stations, named A, B and C. The coring stations are 25 km apart from each other and form a triangle that is at the greatest distance from the nearest landmasses. The sediments consist of foraminifer–pteropod oozes (layers U1 and U4 from bottom to top), two pteropod oozes (U2 and U5) and a turbidite layer (U3). The same sequence has been identified in the three cores.

The turbidite layer U3 that lies on top of U2 (^{14}C AMS dated at 1814 cal yrs BP) ranges from 5 to 11 cm thick and is clearly distinguished from the dominating hemipelagic sediments by colour variations, higher water content and the absence of planktonic foraminifer shells. Rather uniform values of organic carbon and nitrogen are also characteristic of the U3 turbidite unit, likely because of homogenisation during transport and emplacement. In addition, U3 unit shows higher contents of terrigenous elements such as K and Fe. Otherwise, the presence of zeolites in the turbidite layer supports the hypothesis of the Sardinian continental margin, where pyroclastic deposits are known, as the most likely source area for U3. Our results demonstrate the ability of turbidity currents originating on the margins surrounding the Balearic Abyssal Plain to reach the very centre of the basin during high sea level still stands as the present one.

Keywords: Balearic Abyssal Plain; Late Holocene; hemipelagic sedimentation; turbidite deposits

1. Introduction

Most of the studies on the sedimentation of fines during the Holocene in the Western Mediterranean Sea have been performed in slope and rise environments of the Gulf of Lions, the Catalan and the Balearic margins, and the Alboran Sea (Buscail et al., 1997; Zuo et al., 1997; Sanchez-Cabeza et al., 1999; Giresse et al., 2001; Accornero et al., 2003; Masqué et al., 2003). One of the aims of those studies was testing the likely funnelling effect of submarine canyons for sediment transport if compared with open slope settings (Durrieu de Madron et al., 2005; Palanques et al., 2006).

Corresponding author: Tel.: +34 934021361; fax: +34 934021340.
E-mail address: antonicalafat@ub.edu (A. Calafat).

While constituting the dominant sedimentary environment in the Western Mediterranean, abyssal plains are viewed as typical hemipelagic settings with low sedimentation rates where sediment supply is dominated by pelagic and aeolian inputs (Guerzoni et al., 1997; Guieu et al., 1997, Zuo et al., 1997). However, some authors have shown that sediment gravity flows triggered by mass wasting events on the basin margins reached the abyssal plain environment during pre-Holocene times. Such events resulted in centimetre to metre thick layers of allochtonous materials (Morris et al., 1998; Rothwell et al., 1998; Hoogakker et al., 2004). A ~22 000 yr BP pre-Holocene megaturbidite, representing a volume of about 600 km^3 of sediment, was identified by Rothwell et al. (2000) in the Balearic Abyssal Plain (BAP). Sandy turbidites have equally been reported along the eastern edge of the BAP (Kenyon et al., 2002).

Though it is generally thought that mass failure and turbidite events mostly occur during sea level lowstands (Posamentier et al., 1998), they may occur at any time since their triggering mechanisms are controlled by factors other than sea level (Droz et al., 2001; Dennielou et al., 2003; Bonnel et al., 2005).

By contrast with the above mentioned studies, the potential occurrence of turbidite deposits of Late Holocene age in the deep basins of the Mediterranean Sea has received little attention to date. Several authors have already shown that a number of sedimentological and geochemical properties are particularly useful to distinguish fine-grained turbidites from hemipelagic deposits in abyssal plain settings (Colley et al., 1984; Thomson et al., 1987; Grantz et al., 1996).

The aim of our study was performing a high-resolution analysis of the Late Holocene sediment record from the deepest and most distal part of the BAP using sedimentological, geochemical and mineralogical proxies, and determining the sources and transport paths of the youngest turbidite deposit in the BAP centre.

2. Physiographic setting

With an extension of 77 000 km^2 and a maximum depth of approximately 2900 m, the Algero–Balearic Basin (ABB) is bounded, in an anti-clockwise direction, by the Balearic Promontory, the SE Iberian margin, the Oran Rise, the North-African margin, the Tyrrhenian Though, the Corsica–Sardinia block, the Ligurian Sea, the Gulf of Lion and the Valencia Though (Fig. 1). The BAP is the central, deepest part of the ABB in between the Balearic Promontory and the mouth of the Valencia Though, and the Sardinia–Corsica block (Fig. 1). The continental shelves surrounding the deep basin have widths ranging from 200 km in the Gulf of Lion to 30–50 km west of Corsica and Sardinia to 20–54 km off North Africa. The main sediment sources are the Rhône and the Ebro rivers (UNEP/MAP/MED POL, 2003). They have formed the widest, prograding continental shelves and slopes in the Western Mediterranean Sea. An

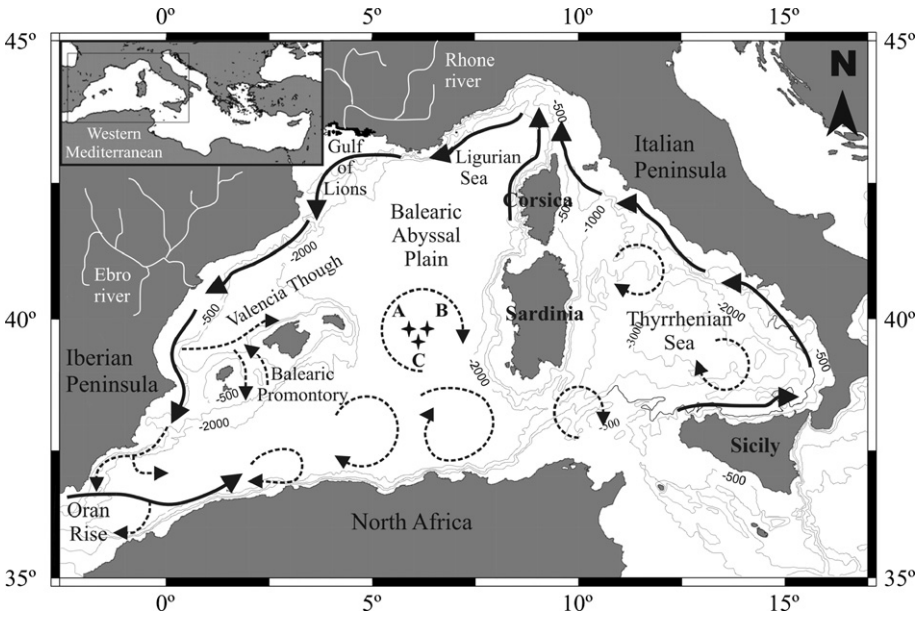

Fig. 1. Location of cores A, B and C in the Balearic Abyssal Plain and, general physiographic setting and superficial circulation patterns (modified from Millot, 1987) of the Western Mediterranean Sea. Distance between stations is not in accord with the map scale.

Table 1
Location and length of the sediment cores from the Balearic Abyssal Plain investigated in this study

Core	Sampling date	Location		Water depth (m)	Length core (cm)
		Longitude	Latitude		
A	14/03/01	39°28.30′ N	5°57.37′ E	2850	22
B	13/02/01	39°29.51′ N	6°10.88′ E	2854	30
C	13/03/01	39°18.81′ N	6°04.22′ E	2854	30

intricate network of submarine canyons cuts the Rhône-Gulf of Lion slope and outer shelf (Droz, 1983; Canals, 1985; Bellaiche et al., 1986). The continental margin west of Corsica and Sardinia is not only much narrower but steeper than the Rhône-Gulf of Lion margin. It is incised by short, steep submarine canyons connected directly to torrents inland (Shepard, 1972; MediMap Group, 2005). The North African continental margin is not only narrow but seismically active. The slope there displays a complex topography with short submarine canyons as a consequence of its collisional tectonic setting (Domzig et al., 2006).

3. Oceanographic setting

The oceanographic regime in the Western Mediterranean upper layers is dominated by the input of Modified Atlantic Water (MAW; $S<37.5$), which extends from the surface down to 100–200 m depth, approximately (Millot, 1987). East of the Alboran Sea the main MAW flow forms the Algerian Current that moves eastwards along the North African margin. The Algerian Current commonly forms coastal eddies, 50–100 km in diameter (Millot et al., 1990; Fuda et al., 2000), which spread northwards towards the basin centre. The intermediate depths (300–750 m) are occupied by the Levantine Intermediate Water (LIW; $S>38.5$) that originates in the Eastern Mediterranean and flows westwards to the Gibraltar Strait. The Tyrrhenian Deep Water (TDW) is injected into the ABB at 800–1500 m between the LIW and the Western Mediterranean Deep Water (WMDW) (Rhein et al., 1999). The WMDW ($S\sim38.4$) fills the western basin at depths in excess of 1500 m (Send et al., 1999). The WMDW forms in the Gulf of Lion and the Ligurian Sea during strong, cold and persistent wind events and flows southerly into the ABB (Millot, 1987).

4. Methodology

Three high quality multicores, named A, B and C (Fig. 1, Table 1), were collected from the deepest, central part of the BAP at 2850 m of water depth during a cruise on board *R/V Urania* in March 2001. The

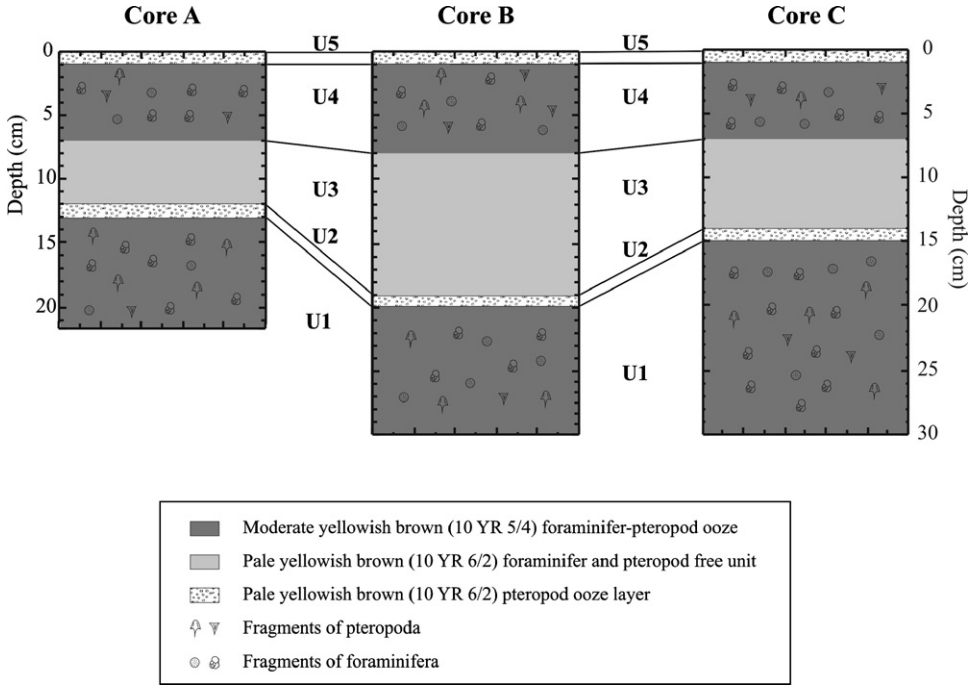

Fig. 2. Logs of cores A, B and C showing lithological units U1 to U5.

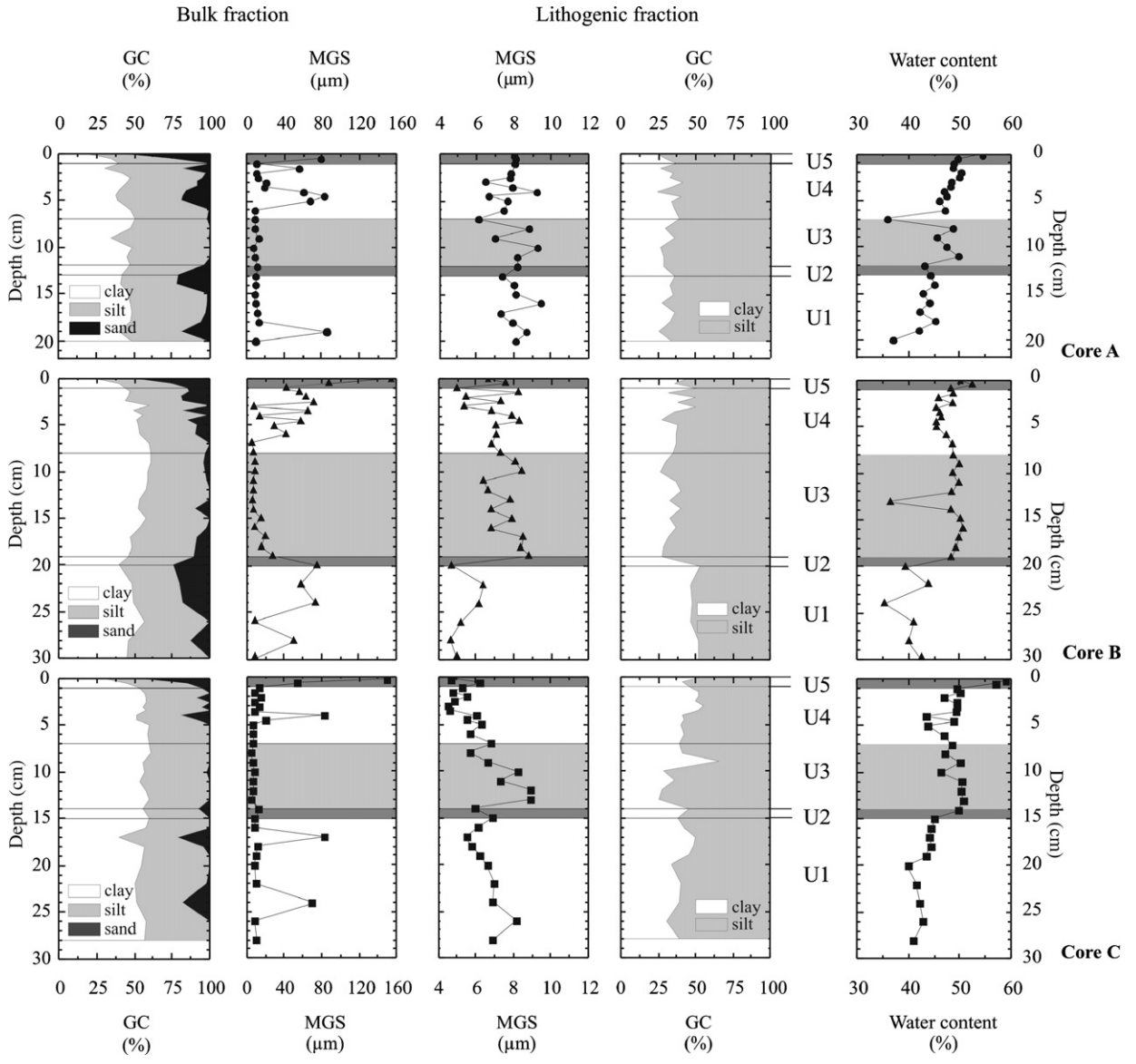

Fig. 3. Vertical profiles of bulk fraction and lithogenic fraction mean grain size (MGS) and granulometric composition (GC) (expressed as percentage of clay, silt and sand) of the sedimentary units identified in cores A, B and C. Also water content profiles are shown for each core.

coring stations occupied the vertex of a 25 km per side triangle (Fig. 1). Two cores from each cast were visually described and sliced into 0.5 to 2 cm thick samples that were stored in sealed plastic bags at 4 °C until processing in the laboratory.

Water content was measured on samples dried at 50 °C until reaching constant weight. At each level, two non-homogenized sub-samples of approximately 1 g each were used for grain size analysis with an LS100 Coulter Counter. The lithogenic material was described from sub-samples treated with 10% H_2O_2 and 1 M HCl to remove organic matter and carbonates, respectively. Biogenic coarse grains were determined on the second set of subsamples after treatment with 10% H_2O_2. Three main grain size categories were considered: i) sand (>63 μm), ii) silt (4–63 μm) and iii) clay (<4 μm), and the mean grain size was calculated for both the bulk sediment and the lithogenic fraction.

Total and organic carbon (C_{total} and C_{org}) and nitrogen were measured on 20–30 mg fractions of non-treated and 25% HCl treated sediment samples after homogenization with an agate mortar. Analytical results from an

Elemental Analyzer CE 2100 were used to calculate organic matter ($C_{org} \times 2$) and calcium carbonate ($[C_{total} - C_{org}] \times 8.33$) contents, and C_{org}/organic nitrogen (N_{org}) ratios following Masqué et al. (2003).

Major elements (Al, P, K, Ca, Si, Ti, Mn, Fe, Na and Mg) were analyzed by X-Ray fluorescence with a Phillips PW 2400 sequential wavelength dispersive X-ray spectrometer on 0.3 g bulk sediment aliquots homogenised with 5.7 g of lithium tetraborate (dilution 1/20). Prior to the analyses, subsamples were casted into fused beds in an induction oven at 1150 °C by addition of 5 mg of a tensoactive compound. As bulk analyses do not reveal which sedimentary fraction adds to the concentration of a particular element, aluminium normalized elemental concentrations were used to analyze changes in the composition of sediments without $CaCO_3$ masking effects (Schnetger et al., 2000).

Bulk sediment XRD mineralogical analyses were carried out on all the sub-samples from core C following Kübler (1987), Adatte et al. (1996) and Tamburini et al. (2003). Bulk sample random powder was used to determine the total mineralogical composition with a SCINTAG XRD 2000 diffractometer. Clay mineralogy analyses were made according to Tamburini et al. (2003).

^{14}C AMS dating was performed on four core C subsamples from which 15 mg of the planktonic foraminifera *Universa orbulina* were extracted from the >150 μm size fraction. Samples were sent to the National Ocean Sciences Accelerator Mass Spectrometer (NOSAMS)

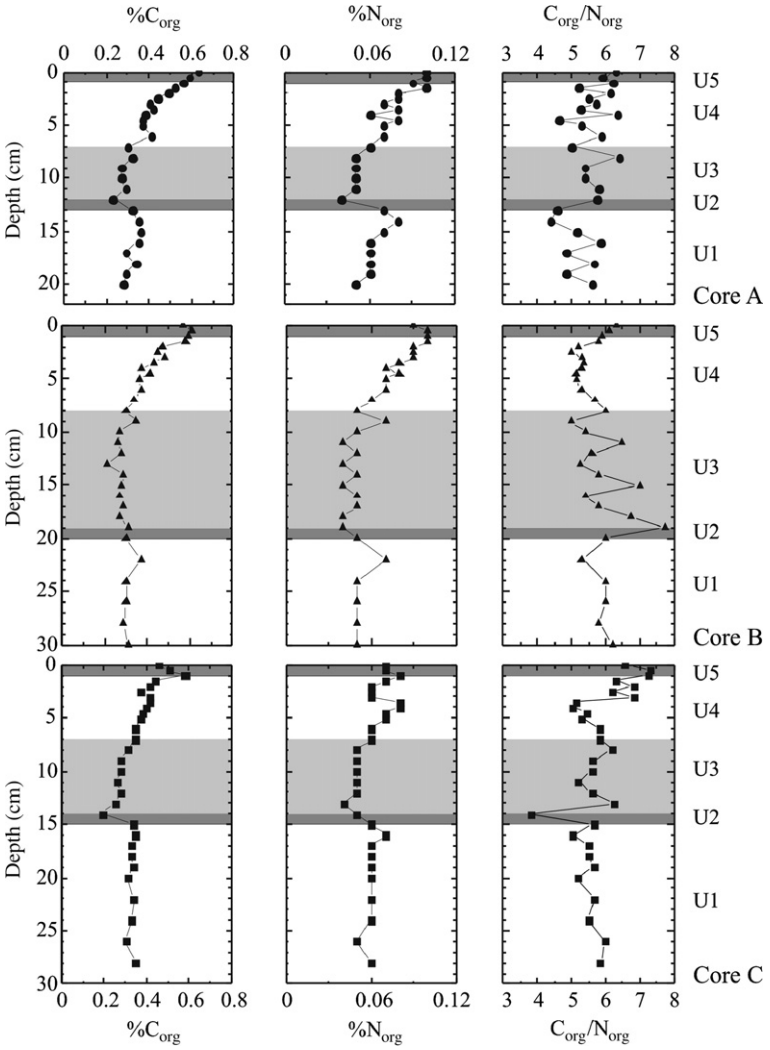

Fig. 4. C_{org}, N_{org} and C_{org}/N_{org} ratio depth profiles of cores A, B and C. The sedimentary units identified in the cores are also shown.

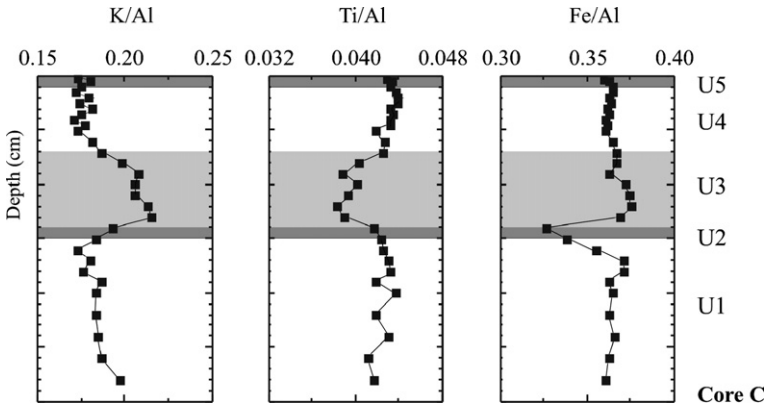

Fig. 5. K/Al, Ti/Al and Fe/Al profiles of core C. The sedimentary units identified in this core are also shown.

facility at Woods Hole, USA. Radiocarbon ages were calibrated with the CALIB V.5.0.2 software. Data are reported with a 2σ uncertainty.

5. Results

5.1. Sediment physical properties

Five sedimentary units were identified in each of the cores, named U1, U2, U3, U4 and U5 from bottom to top (Fig. 2). Units U1 and U4 consist of moderate yellowish brown (10 YR 5/4) foraminifer–pteropod oozes that lie below 1 cm thick pteropod ooze units U2 and U5, respectively. Unit U3 is made of pale yellowish brown (10 YR 6/2) mud with no foraminifera nor pteropod shells. U3 thickness ranges from 5 to 11 cm, and is separated from U2 by a sharp colour contrast at 7 to 8 cm of core depth.

The grain-size analyses carried out in both the bulk and the lithogenic fraction of the sediment (Fig. 3) reveal some clear differences between them. The bulk fraction is composed of clay, silt and bioclastic sand, the latter mainly in the pteropod ooze U5 (41%, 37% and 30% of sand in cores A, B and C, respectively) and at the base of U2 (20% and 24% of sand in cores A and B, respectively) (Fig. 3). All cores show that the mean grain size markedly changes from one level to another within the foraminifer–pteropod ooze units U1 and U4 reflecting the scattered distribution of sand-sized shells and biogenic debris (Fig. 3), while in unit U3 mean grain size values are finest and more homogeneous due to the absence of sand sized biogenic particles (Fig. 3). On the other hand the lithogenic fraction of the sediment show in all cases that the studied sediments are composed by fine-grained pelagic marls rich in silt fraction, ranging between a minimum value of 34% in core C and a maximum value of 75% in core A (Fig. 3). Sands are totally lacking in the lithogenic fraction, which mean grain size ranges from 6.3 to 7.9 μm for the entire cores. Vertical profiles show that a fining upwards sequence exists in unit U3 of the cores B and C (Fig. 3).

The water content roughly increases from core bottom to core top, ranging from 35% at 24 cm depth in core B (unit U1) to 60% at the top of core C (unit U5) (Fig. 3).

Table 2
Elementary correlation matrix for core C (r coefficient)

	Fe	Mn	Ti	Ca	K	Si	Al
Fe	1						
Mn	0.445	1					
Ti	**0.757**	0.231	1				
Ca	−0.723	−0.529	−0.639	1			
K	0.379	0.397	−0.197	−0.408	1		
Si	**0.937**	0.352	**0.884**	−0.728	0.187	1	
Al	**0.923**	0.386	**0.888**	−0.775	0.225	**0.983**	1

Bold numbers show the higher (r>0.75) positive correlations between the major elements.

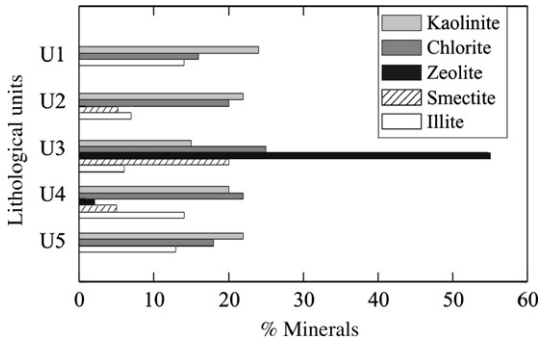

Fig. 6. Fine fraction minerological composition of the sedimentary units U1 to U5 in core C. Kaolinite, clorite and zeolite percentages were obtained from the analysis of the coarse clay–fine silt 2–16 μm fraction while smectite and illite percentages were derived from the analysis of the clay <2 μm fraction of the sediment samples.

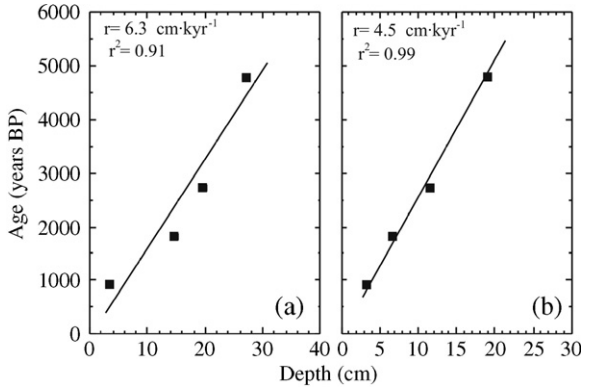

Fig. 7. Age model of core C from ^{14}C calibrated ages. In (a) the presence of the turbidite unit U3 is not considered. Therefore, dating points from both units U2 and U1, corresponding to 14–15 cm, 19–20 cm and 26–28 cm core depths have been shifted 7 cm upcore. In (b) the turbidite unit between 7 and 14 cm core depth is computed.

However, such general tendency is punctuated by a marked jump from U2 to the foraminifer–pteropod free unit U3 that shows relatively high water contents (Fig. 3).

5.2. Sediment composition

The vertical profiles of C_{org} and N_{org} abundances are shown in Fig. 4. C_{org} and N_{org} contents range from 0.19% to 0.63% and from 0.04% and 0.1%, respectively. These are values typical of ocean regions with low autochthonous primary productivity like the ABB (Bosc et al., 2004), and are much lower than those recorded in other Western Mediterranean areas with well developed density fronts and nearby river discharges that fertilize the surface waters, like the Alboran Sea (0.5–1.5%) (Masqué et al., 2003) and the Gulf of Lions (0.6–0.9%) (Giresse et al., 2001). The highest values of both C_{org} and N_{org} correspond to the uppermost unit U5 (Fig. 4). From that point both parameters display a decreasing trend with depth with the values within the lowermost unit U1 being more constant (Fig. 4). The passage from U1 to U3 through U2 is marked by a diminution in both C_{org} and N_{org} contents (Fig. 4).

C_{org}/N_{org} ratios shift less than 4 units overall (3.8 to 7.8). The highest variability usually corresponds to U3. In the lower foraminifer–pteropod ooze unit U1, the C_{org}/N_{org} ratio remains fairly constant in cores B and C (Fig. 4).

Major elements/Al ratios were determined in core C and some of them are presented in Fig. 5. A correlation matrix between those elements shows their main relationships (Table 2). Ca, representing the biogenic pelagic source, is negatively correlated with all the other elements. Al, Ti, Si and Fe, representing the continent-derived silicate fraction of the sediments (Schnetger et al., 2000), show high correlation coefficients (Table 2).

In general, the values of the various ratios remain fairly constant except in the foraminifer–pteropod free unit U3. Unit U3 recorded the highest K/Al and Fe/Al, and the lowest Ti/Al values (Fig. 5). The K/Al ratio clearly follows the mean lithogenic grain size record with the highest value (0.215) in U3 where the lithogenic fraction is coarser (Figs. 3 and 5). The Fe/Al ratio is fairly constant with the exception of a spike centered in U2. Also, a slight increase was found in U3.

The clay mineral composition of the various units was also determined in core C (Fig. 6). The foraminifer–pteropod and pteropod oozes U1, U2, U4 and U5 mainly consist of kaolinite (20%–24%), chlorite (16%–22%) and illite (7%–14%). In the foraminifer–pteropod free unit U3, kaolinite and chlorite represent 15% and 25% of the total clay content, respectively. In addition, smectite is an abundant clay mineral within U3, with contents of up to 20% of the total clay. A distinctive characteristic of unit U3 is the presence of zeolite in the coarse clay–fine silt 2–16 μm fraction, with contents as high as 82% at 12 cm core depth. Zeolite, an alteration product of volcanic minerals (Bogaard et al., 1999), is absent from the other sediment units in the studied cores.

5.3. ^{14}C dating

Core C ^{14}C dating results are shown in Fig. 7 and Table 3. An integrated sediment accumulation rate (SAR) of 6.3 cm kyr^{-1} from core base to top was

Table 3
(a) ^{14}C AMS ages of core C performed on the planktonic foraminifer *Universa orbulina*; (b) sediment accumulation rates (SAR) derived from linear regression of ^{14}C calibrated ages from core C

(a)

Units	Section (cm)	^{14}C age (yr BP)	$\delta^{13}C$	Calibrated age (yr BP)	
U4	3.0–3.5	1390±40	2.39	939	+1043–834
U2	14–15	2220±40	2.34	1814	+1922–1705
U1	19–20	2960±30	2.19	2747	+2810–2683
	26–28	4590±40	2.21	4802	+4927–4677

(b)

Units	Section (cm)	SAR (cm kyr^{-1})
U5/U4	0–3.5	3.7
U3/U2	3.5–15	13.1
U1	15–19	4.3
U1	19–28	4.4

Note: BP:1950 AD.

calculated from linear regression of the age model (Fig. 7a). Two samples from within unit U1 gave ^{14}C ages of 4802 cal yr BP (26–28 cm core depth) and 2747 cal yr BP (19–20 cm core depth), respectively. The resulting SAR in this lower foraminifer–pteropod ooze U1 is then 4.4 cm kyr^{-1}. The pteropod ooze unit U2 at 14–15 cm core depth gave a ^{14}C age of 1814 cal yr BP at 14–15 cm core depth. U3 could not be ^{14}C dated because of the lack of foraminifera. The 3–3.5 cm core depth sample within U4 yielded a ^{14}C age of 939 cal yr BP thus providing a SAR of 3.7 cm kyr^{-1} for the uppermost core section (Table 3b). From those numbers, a higher SAR (13.1 cm kyr^{-1}) results for the 3.5–15 cm interval including unit U3. However, it is likely that the actual SAR of U3 was much higher since the former values result from interpolation of two datings on pelagic oozes U2 and U4. With the exception of the interval containing foraminifer and pteropod free U3 unit, the SAR obtained are slightly lower than the ones (5.7–7.8 cm kyr^{-1}) given by Weldeab et al. (2003) for the ABB.

6. Discussion

Since the late 1970's it has been generally admitted that abyssal plains receive enhanced sediment inputs during sea level lowstands when rivers discharge their sediment load near the shelf edge or directly into submarine canyon heads from where it is funnelled beyond continental margins (Vail et al., 1977; Miller et al., 1987; Posamentier et al., 1998; Dennielou et al., 2003; Bonnel et al., 2005). The delivery rate of particles from sea surface productivity and aeolian inputs responds as well to global climatic oscillations, that had a strong impact on the Western Mediterranean (Moreno et al., 2002; Martrat et al., 2004). This sediment input variability is better known for pre-Holocene times than in the Holocene period. This is partly because the available data set on Late Holocene sediments in abyssal plains is derived mainly from piston and gravity cores with poor quality recovery of the youngest, softer sedimentary material that is often lost during coring. Multicoring looks as the best option to recover short, high quality cores of Late Holocene age from abyssal plain settings.

6.1. Hemipelagic and turbiditic sedimentation

In the BAP, Late Holocene sediments consist mostly of hemipelagic foraminifer–pteropod oozes and pteropod oozes typical of deep ocean settings above the calcite compensation depth where the C_{org}/N_{org} ratio varies no more than 4 units (Fig. 4), thus showing the dominance of marine above terrestrial organic matter (Buscail et al., 1997). However, fine particle funnelling along submarine canyons and the carrying capacity of the WMDW flowing to the south (Rhein et al., 1999) likely constitute efficient mechanisms of transport and delivery of suspended sediment to the deep basin. Intermediate nepheloid layers to which pteropoda are probably associated could explain the formation of the well preserved pteropod unit after quick settling following nepheloid layer collapse. Such hypothesis can explain the shift in C_{org} contents above and below U2 in cores A and C (i.e. from 0.19% at the base of U3 to 0.34% at the top of U1 in core C) (Fig. 4), interpreted as a consequence of the quick deposition of the pteropod ooze U2 (and possibly U3) that cut the oxygenation of the underlying unit U1, and thus preserves the organic matter as indicated by the higher organic carbon concentrations in that unit with respect to U2 and U3 (Fig. 4).

However, in this framework, the various proxies analyzed show that such hemipelagic foraminifer/pteropod oozes are perturbed by the deposition of a base cut-out fine-grained turbidite (unit U3) ranging in thickness from 5 cm in core A to 11 cm in core B (Fig. 2). The wideness of the BAP and the absence of lateral confinement may cause turbidite deposits to spread over large areas as illustrated by "Rothwell's megaturbidite" that covers 77 000 km^2 of the BAP (Rothwell et al., 2000). According to Hoogakker et al. (2004) about 90% of the sedimentary sequence of the BAP would consist of turbidites that are clearly distinguishable from the intercalated hemipelagic intervals based on colour variations, sedimentary structures and foraminifera content.

The deposition of turbidites is considered as an instantaneous event that will disrupt the otherwise low sediment accumulation rates of pelagic and hemipelagic sediments. In core C, if the turbidite unit U3 is excluded, the resulting overall accumulation rate derived from AMS ^{14}C calibrated ages is 4.5 cm kyr^{-1} (Fig. 7b). If U3 is integrated in the calculations then the SAR for the entire section rises to 6.3 cm kyr^{-1} (Fig. 7a), that is 1.5 times higher. SAR calculated from linear regressions of the age-depth curves show that in the 3–15 cm intervals which includes the turbidite unit U3, the overall sedimentation rate (13.1 cm kyr^{-1}) is much higher than in the hemipelagic intervals above and below (Table 3b).

Several authors (Mulder et al., 2001; Hoogakker et al., 2004) consider that the deposition of deep-sea turbidites leads to relative enrichments in siliciclastic grains because of particle sorting. This would explain the upwards shift of the mean grain size in the lithogenic

fraction at the base of the turbidite unit U3 as observed in cores B and C (Fig. 3). It is unknown to which extent the pteropod unit U2 was disrupted by the emplacement of U3, but the lack of pteropod debris within U3 suggests that disruption was minimal, therefore pointing to low density, low turbulence conditions. This may correspond to the distal part of a turbidity surge that would have released its coarsest load in more proximal positions, where turbulence was likely higher. Furthermore, the absence of pelagic organisms inside U3 supports the idea of a relatively fast emplacement of the sediments. The higher water content and lower organic carbon and organic nitrogen concentrations in U3 with respect to the underlying and overlying sediments (Figs. 3 and 4) is likely related to a different origin of the material forming unit U3.

Such different origin of the unit is further supported by the geochemical signature of the sediments. The concentration/depth profiles of non-reactive elements such as K, Ti and Fe can be used as tracers of turbidite deposition (Thomson et al., 1998). In U3 the profiles of these elements roughly parallel (i.e. K/Al) or mirror (i.e. Ti/Al) the size-graded distribution of the mean lithogenic grain size (Figs. 3 and 5). Variations in these elemental ratios have been attributed to changes in clay mineralogy and to the effects of particle sorting (Shimmield and Mowbray, 1991). The increase of the K/Al ratio in U3 is interpreted as an enrichment of the terrigenous clay mineral content (Weedon and Shackleton, 1997; Moreno et al., 2002). The base of the turbidite unit U3 is clearly distinguishable by the relatively high value of the K/Al ratio (0.215) as compared to the hemipelagic oozes mean value (0.176).

As a refractory element, Ti resides within heavy minerals, and within clay minerals (Weedon and Shackleton, 1997) and is often associated to aeolian sediments like loess and Saharan dust (Wehausen and Brumsack, 1999; Moreno et al., 2002). The diminution of the Ti/Al ratio within the turbidite unit U3 (Fig. 5) is an indicator of the relative decrease of aeolian-transported heavy minerals in the lithogenic fraction (Shimmield and Mowbray, 1991). Finally, the good correlation of Fe with other siliciclastic elements such as Al ($r=0.923$) and Si ($r=0.937$) (Table 2) demonstrates that Fe contents are essentially supplied in detrital form by the continental margins surrounding the BAP (Marin and Giresse, 2001).

6.2. Provenance of the turbiditic materials

Identifying the provenance of the materials forming the turbidite unit U3 may help to better understand the sedimentary functioning of the BAP during sea level high stands, like in the Late Holocene. Previous studies have shown extensive turbidite deposition and large-scale bedforms along the outer rim of the BAP and beyond that were attributed to sediment inputs mainly from the Rhône river and the NE Iberian rivers (Morris et al., 1998; Rothwell et al., 2000; Dennielou et al., 2003; Hoogakker et al., 2004) but also from the Corsican and Sardinian margins where submarine canyons are efficient in funnelling sediments to the continental rise (Got and Aloisi, 1990; Kenyon et al., 2002).

Clay minerals may be good indicators of the formation environment of sedimentary units, and clay mineral assemblages in marine sediments are useful tracers of detrital sources, dispersal patterns, past and recent sedimentary conditions and alteration processes (Chamley, 1989). The clay mineral fraction of the surface sediments of the BAP is mainly composed by: i) illite and chlorite derived from the Rhône and Ebro rivers, and ii) clay minerals from the aeolian dust, which may be dominated either by smectite, if derived from Morocco and Western Algeria, or kaolinite and palygorskite, if coming from the Algeria/Tunisia area and the Saharan desert (Hoogakker et al., 2004). Illite and kaolinite have been reported as the most abundant clay minerals in the Algerian continental shelf (Leclaire, 1972).

In our cores, two main groups of clay minerals have been distinguished (Fig. 6). The first group includes kaolinite, chlorite and illite and is present in both the hemipelagic and turbidite units. The decrease of the kaolinite content in unit U3 (Fig. 6) correlates with the relative decrease of aeolian-transported Ti-enriched heavy minerals of the siliciclastic fraction (Hoogakker et al., 2004) (Fig. 6). The presence of substantial amounts of illite and chlorite in all units (Fig. 6) shows the efficient transfer of terrigenous materials from the river-fed continental margins to the north of the BAP during the Late Holocene, thereby contributing to the background pelagic sediment flux.

The second group of minerals is composed of smectite and zeolite that show relatively higher abundances in the turbidite unit U3 (Fig. 6). The smectite content in U3, reaching a maximum value of 20% at 13–14 cm core depth, could be initially attributed to a significant contribution of aeolian dust from western North Africa. However, the kaolinite/chlorite ratio in such unit U3 is lower than it should be for a North African source, >2 according to Guerzoni et al. (1997). Therefore, the origin of the clay particles in U3 cannot be aeolian. An alternative explanation could be the transport to the BAP of smectite from Italian rivers (Foucault and Melières, 2000) opening into the Tyrrhenian Sea by the intermediation of LIW and TDW flows. However, such

an input cannot be major and the process responsible for the quick and massive transfer of material eventually leading to the formation of U3 remains unidentified.

The zeolite and smectite contents of U3 are best explained if a suitable volcanoclastic source is identified on the margins of the BAP. The Balearic Promontory is excluded as a potential source since studies carried out by Alonso et al. (1998) and Fornos (1987) described the superficial sediments as carbonatic materials dominated by the presence of bioclastic sands and lithic fragments. Only Cerri et al. (2001) showed Oligo–Miocene volcanoclastic deposits along the western coast of Sardinia, which were easily transformed into zeolitized units shortly after their deposition. Since zeolite is diagnostic of the turbidite unit U3, we suggest that reworking of a sedimentary unit in the Sardinian margin containing materials resulting from the degradation of volcanoclastics led to the formation of the central BAP turbidite U3. In addition, Cerri et al. (2001) also considered that within the zeolitized units of the western coast of Sardinia, clinoptilolite constitutes the cement deriving from the transformation of the precursor rhyolitic glass. This fact would explain the enrichment in the K/Al ratio founded in the turbidite unit U3 (Fig. 5) since the authors considered that clinoptilolite is associated to high potassium contents.

The existence of this central BAP turbidite implies a run out of approximately 120 km on slope gradients of less than 0.02° along most of the transport path. The graded intervals within U3 (i.e. mean grain size of the lithogenic fraction in core C, Fig. 3), the poor sorting of the volcanoclastic-derived materials and the fact they appear clearly reworked with other terrigenous materials such as illite and chlorite reinforces the interpretation of U3 as the result of a turbidite current. The thickness of U3 provides additional clues about its source area. The maximum thickness (11 cm) corresponds to core B, which is the closest station to the hypothesized source area in Sardinia. Kenyon et al. (2002) showed that the fine-grained portion of upper slope sediments from the Corsica and Sardinia margins is underrepresented on canyon-mouth lobes. These authors thought that the fine fraction had been likely transported beyond canyon mouths to contribute to the development of the turbidite succession of the BAP. Therefore, the observations by Kenyon et al. (2002) further support our interpretation.

7. Conclusions

Late Holocene sediments recovered in the central part of the Balearic Abyssal Plain consist of foraminifer–pteropod oozes and pteropod oozes interrupted by a 5–11 cm thick turbidite unit U3 on top of a pteropod ooze unit with a ^{14}C AMS age of 1814 cal yr BP. Datings of hemipelagic materials above and below the turbidite unit demonstrated higher sediment accumulation rates in this unit than in the hemipelagic intervals.

The turbidite unit is clearly distinguishable from grain size, both organic carbon and organic nitrogen contents, geochemical composition and mineralogical criteria. It is lighter coloured, has higher water content and contains less organic carbon than the hemipelagic units. The very low content of biogenic sand grains of pelagic origin, and the higher mean grain size of the lithogenic fraction further support the turbiditic character of this unit.

While the chemically inert elements do not show significant variations in the hemipelagic intervals, shifts associated to the turbidite sediments were observed as illustrated by higher K/Al and lower Ti/Al ratios. The presence of volcanoclastic zeolites (clinoptilolite) in the turbidite unit points to the western margin of Sardinia as the most likely source area. It is hypothesized that the zeolitized units in the source area were reworked and deposited in the deepest part of the BAP as an admixture of terrigenous material carried by a turbidity current with a run-out of at least 120 km on an almost totally flat seafloor.

The centimetre thick pteropod ooze layer on top of which the turbidity unit lies was not disturbed by the emplacement of the turbidite deposit, therefore pointing to the tail of a turbulent surge depositing a base-cut-out turbidite.

Our results demonstrate that terrigenous materials from the basin margins may be efficiently transferred to the deepest parts of the Balearic Abyssal Plain, even during high sea-level periods like the Late Holocene.

Acknowledgements

The authors thank the officers and crew of *R/V Urania* for their technical support during sea work (March and April 2001). We also thank the Laboratory of Sedimentology and the Scientific–Technical Services of the University of Barcelona for their help with the sedimentological and geochemical analyses. We gratefully acknowledge the support of the US National Science Foundation for the ^{14}C dating of sediment samples at NOSAMS (Woods Hole Oceanographic Institution) and University of Neuchâtel, Switzerland, for mineralogy analyses. The IAEA is grateful for the support provided to its Marine Environment Laboratory by the Government of the Principality of Monaco. This study was supported by the European Commission research projects ADIOS (EVK3-2000-00604), EURO-STRATAFORM (CT-2001-00200) and EURODOM

(RTN2-2001-00281). D. Zúñiga benefited from a Spanish FPU grant (AP2000-0524). GRC Geociències Marines acknowledges support by Generalitat de Catalunya through its excellence research groups programme (ref. 2005 SGR-00152) and the "Barcelona Consortium of Marine Geosciencies" thematic network.

References

Accornero, A., Picon, P., De Bovée, F., Charriere, B., Buscail, R., 2003. Organic carbon budget at the sediment–water interface on the Gulf of Lions continental margin. Cont. Shelf Res. 23, 79–92.

Adatte, T., Stinnesbeck, W., Keller, G., 1996. Lithostratigraphic and mineralogic correlations of near K/T boundary clastic sediments in northeastern Mexico: implications for origin and nature of deposition. Geol. Soc. Am., Spec. Pap. 307, 211–226.

Alonso, B., Guillen, J., Canals, M., Serra, J., Acosta, J., Herranz, P., Sanz, J.L., Calafat, A., Catafau, E., 1998. Los sedimentos dela plataforma continental balear. Acta Geol. Hisp. 23, 185–196.

Bellaiche, G., Coutellier, V., Droz, L., 1986. Seismic evidence of widespread mass transport deposits in the Rhône deep-sea fan: their role in the fan construction. Mar. Geol. 71, 327–340.

Bogaard, P., Mocek, B., Stavesan, M., 1999. Chronology and composition of volcanoclastic ash layers in the central Tyrrhenian Basin (site 974). Proc. Ocean Drill. Program Sci. Results 161, 137–156.

Bonnel, C., Dennielou, B., Droz, L., Mulder, T., Berné, S., 2005. Architecture and depositional pattern of the Rhône Neofan and recent gravity activity in the Gulf of Lions (western Mediterranean). Mar. Pet. Geol. 22, 827–843.

Bosc, E., Bricaud, A., Antoine, D., 2004. Seasonal and interannual variability in algal biomass and primary production in the Mediterranean Sea, as derived from 4 years of SeaWiFS observations. Glob. Biogeochem. Cycles 18, 2003–2034.

Buscail, R., Ambatsian, P., Monaco, A., Bernat, M., 1997. 210Pb, manganese and carbon indicators of focussing processes on the northwestern Mediterranean continental margin. Mar. Geol. 137, 271–286.

Canals, M., 1985. Estructura sedimentaria y evolución morfológica del talud y el glacis continentales del Golfo de León: Fenómenos de desestabilización de la cobertura sedimentaria plio-cuaternaria (Ph.D. thesis), Barcelona, Universitat de Barcelona, pp. 215–226.

Cerri, G., Cappelletti, P., Langella, A., De'Gennaro, M., 2001. Zeolitization of Oligo–Miocene volcanoclastic rocks from Logudoro (northern Sardinia, Italy). Contrib. Mineral. Petrol. 140 (4), 404–421.

Chamley, H., 1989. Clay Sedimentology. Ed. Springer-Verlag, Berlin Heidelberg, pp 621.

Colley, S., Thomson, J., Wilson, T.R.S., Higgs, N.C., 1984. Post-depositional migration of elements during diagenesis brown clay and turbidite sequences in the North East Atlantic. Geochim. Cosmochim. Acta 48, 1223–1235.

Dennielou, B., Bonnel, C., Sultan, N., Voisset, M., Berné, S., Droz, L., 2003. Sand transfer into the deep basin of the Gulf of Lions even during the sea level high stand. Ocean Margin Research Conference, September 15th–17th 2003, Paris, p. 129.

Domzig, A., Yelles, K., Le Roy, C., Déverchère, J., Bouillin, J.P., Bracène, R., Mercier de Lépinay, B., Le Roy, P., Calais, E., Kherroubi, A., Gaullier, V., Savoye, B., Pauc, H., 2006. Searching for the Africa–Eurasia Miocene boundary offshore western Algeria (MARADJA'03 cruise). C. R. Geosci. 338, 80–91.

Droz, L., 1983. L'eventail sous-marin profond du Rhône (Golfe du Lion): grands traits morphologiques et structure semi-profonde. 3rd cycle Thesis, Paris VI University, 195 pp.

Droz, L., Kergoat, R., Cochonat, P., Berné, S., 2001. Recent sedimentary events in the western Gulf of Lions (Western Mediterranean). Mar. Geol. 176, 23–37.

Durrieu de Madron, X., Ferré, B., Le Corre, C., Grenz, P., Conan, M., Pujo-Pay, M., Buscail, R., Bodiot, O., 2005. Trawling-induced resuspension and dispersal of muddy sediments and dissolved elements in the Gulf of Lions (NW Mediterranean). Cont. Shelf Res. 25 (19–20), 2387–2409.

Fornos, J.J., 1987. Les plataformes carbonatades de les Balears. Estudi sedimentològic de les plataformes miocenes de les Illes Balears i la comparació amb la sedimentació actual a la seva plataforma. PhD Thesis, Univ. Barcelona, Spain.

Foucault, A., Melières, F., 2000. Paleoclimatic cyclicity in central Mediterranean Pliocene sediments: the mineralogical signal. Palaeogeogr. Palaeoclimatol. Palaeoecol. 158, 311–323.

Fuda, J.L., Millot, C., Taupier-Letage, I., Send, U., Bocognano, J.M., 2000. XBT monitoring of a meridian section across the western Mediterranean Sea. Deep-Sea Res., Part 1, Oceanogr. Res. Pap. 47, 2191–2218.

Giresse, P., Buscail, R., Charrière, B., Abassi, A., Masqué, P., Sanchez-Cabeza, J.A., 2001. Biotracers and geotracers of depositional events in NW Mediterranean margin over the past two centuries. Oceanol. Acta 24 (6), 581–597.

Got, H., Aloisi, J.C., 1990. The Holocene sedimentation on the Gulf of Lions margin: a quantitative approach. Cont. Shelf Res. 10 (9–11), 841–855.

Grantz, A., Phillips, R.L., Mulen, M.W., Starratt, S.W., Jones, G.A., Sathy Naidu, A., Finney, B.P., 1996. Character, paleoenvironment, rate of accumulation, and evidence for seismic triggering of Holocene turbidites, Canada Abyssal Plain, Arctic Ocean. Mar. Geol. 133, 51–73.

Guerzoni, S., Molinaroli, E., Chester, R., 1997. Saharan dust inputs to the western Mediterranean Sea: depositional patterns, geochemistry and sedimentological implications. Deep-Sea Res., Part 2, Top. Stud. Oceanogr. 44 (3–4), 631–654.

Guieu, C., Chester, R., Nimmo, M., Martin, J.M., Guerzoni, S., Nicolas, E., Mateu, J., Keyse, S., 1997. Atmospheric input of dissolved and particulate metals to the northwestern Mediterranean. Deep-Sea Res., Part 2, Top. Stud. Oceanogr. 44 (3–4), 655–674.

Hoogakker, B.A.A., Rothwell, R.G., Rohling, E.J., Paterne, M., Stow, D.A.V., Herrle, J.O., Clayton, T., 2004. Variations in terrigenous dilution in western Mediterranean Sea pelagic sediments in response to climate change during the last glacial cycle. Mar. Geol. 211 (1–2), 21–43.

Kenyon, N.H., Klaucke, I., Millington, J., Ivanov, M.K., 2002. Sandy submarine canyon-mouth lobes on the western margin of Corsica and Sardinia, Mediterranean Sea. Mar. Geol. 184, 69–84.

Kübler, B., 1987. Cristallinité de l'illite, méthodes normalisées de préparations, méthodes normalisées de mesures. Cahiers Institut Géologie de Neuchâtel, Suisse, série ADX.

Leclaire, L., 1972. La sédimentation Holocèce sur le versant méridional du bassin Algéro-Baléares (Précontinent Algérien). Ed. Du Muséum, Paris, pp. 348–349.

Marin, B., Giresse, P., 2001. Particulate manganese and iron in recent sediments of the Gulf of Lions continental margin (north-western Mediterranean Sea): deposition and diagenetic process. Mar. Geol. 172, 147–165.

Martrat, B., Grimalt, J.O., Lopez-Martinez, C., Cacho, I., Sierro, F.J., Flores, J.A., Zahn, R., Canals, M., Curtis, J.H., Hodell, D.A., 2004. Abrupt temperature changes in the Western Mediterranean over the past 250,000 years. Science 306, 1762–1765.

Masqué, P., Fabrés, J., Canals, M., Sanchez-Cabeza, J.A., Sanchez-Vidal, A., Cacho, I., Calafat, A.M., Bruach, J.M., 2003. Accumulation rates of major constituents of hemipelagic sediments in the deep Alboran Sea: a centennial perspective of sedimentary dynamics. Mar. Geol. 193, 207–233.

MediMap Group, 2005. Morpho-bathymetry of the Mediterranean Sea. CIESM / Ifremer special publication, Atlases and Maps, two maps at 1/2 000 000.

Miller, K.G., Melillo, A.J., Mountain, G.S., Farre, J.A., Poag, C.W., 1987. Middle to Late Miocene canyon cutting on the New Jersey continental slope: biostratigraphic and seismic stratigraphic evidence. Geology 15, 509–512.

Millot, C., 1987. Circulation in the Western Mediterranean Sea. Oceanol. Acta 10 (2), 143–149.

Millot, C., Taupier-Letage, I., Benzohra, M., 1990. The Algerian eddies. Earth-Sci. Rev. 27 (3), 203–219.

Moreno, A., Cacho, I., Canals, M., Prins, M.A., Sánchez-Goñi, M.F., Grimalt, J.O., Weltje, G.J., 2002. Saharan dust transport and high-latitute glacial climatic variability: the Alboran Sea record. Quat. Res. 58 (3), 318–328.

Morris, S.A., Kenyon, N.H., Limonov, A.F., Alexander, J., 1998. Downstream changes of large-scale bedforms in turbidites around the Valencia channel mouth, north-west Mediterranean: implications for paleoflow reconstruction. Sedimentology 45, 365–377.

Mulder, T., Weber, O., Anschutz, P., Jorissen, F.J., Jouanneau, J.-M., 2001. A few months-old storm generated turbidite deposited in the Capbreton Canyon (Bay of Biscay, SW France). Geo Mar. Lett. 21, 149–156.

Palanques, A., Martín, J., Guillén, J., Company, J.B., Sardà, F., 2006. Evidence of sediment gravity flows induced by trawling in the Palamós (Fonera) submarine canyon (northwestern Mediterranean). Deep-Sea Res., Part 1, Oceanogr. Res. Pap. 53 (2), 201–214.

Posamentier, H.W., Jervey, M.T., Vail, P.R., 1998. Eustatic controls on clastic deposition I. In: Wilgus, C.K., Hastings, B.J., Posamentier, H., Van Wagoner, J.C., Ross, C.A., Kendall, C.G.St.C. (Eds.), Sea-level Change: an Integrated Approach. SEPM Spec. Pub., vol. 42, pp. 109–124.

Rhein, M., Send, U., Klein, B., Krahmann, G., 1999. Interbasin deep water exchange in the western Mediterranean. J. Geophys. Res. 104, 23495–23508.

Rothwell, R.G., Thomson, J., Kähler, G., 1998. Low sea-level emplacement of a very large Late Pleistocene megaturbidite in the western Mediterranean Sea. Nature 392, 377–380.

Rothwell, R.G., Reeder, M.S., Anastasakis, G., Stow, D.A.V., Thomson, J., Kähler, G., 2000. Low sea-level stand emplacement of megaturbidites in the western and eastern Mediterranean Sea. Sediment. Geol. 135, 75–88.

Sanchez-Cabeza, J.A., Masqué, P., Ani-Ragolta, I., Merino, J., Frignani, M., Alvisi, F., Palanques, A., Puig, P., 1999. Sediment accumulation rates in the southern Barcelona continental margin (NW Mediterranean Sea) derived from ^{210}Pb and ^{137}Cs chronology. Prog. Oceanogr. 44 (1–3), 313–332.

Schnetger, B., Brumsack, H.-J., Schale, H., Hinrichs, J., Dittert, L., 2000. Geochemical characteristics of deep-sea sediments from the Arabian Sea: a high-resolution study. Deep-Sea Res., Part 2, Top. Stud. Oceanogr. 47, 2735–3768.

Send, U., Font, J., Krahmann, G., Millot, C., Rhein, M., Tintoré, J., 1999. Recent advances in observing the physical oceanography of the western Mediterranean Sea. Prog. Oceanogr. 44, 37–64.

Shepard, F.P., 1972. Submarine canyons. Earth-Sci. Rev. 8 (1), 1–12.

Shimmield, G.B., Mowbray, S.R., 1991. The inorganic geochemical record of the northwest Arabian Sea: a history of productivity variation over the last 400 ky. from Sites 722 and 724. In: Prell, W.L., Niitsuma, N., et al. (Eds.), Proceedings of Ocean Drilling Program. Scientific Results, vol. 117. Ocean Drilling Program, College Station, TX, pp. 409–429.

Tamburini, F., Adatte, T., Föllmi, K., Bernasconi, S.M., Steinmann, P., 2003. Investigating the history of East Asian monsoon and climate during the last glacial–interglacial period (0–140 000 years): mineralogy and geochemistry of ODP Sites 1143 and 1144, South China Sea. Mar. Geol. 201 (1–3), 147–168.

Thomson, J., Colley, S., Higgs, N.C., Hydes, D.J., Wilson, T.R.S., Sørensen, J., 1987. Geochemical oxidation fronts in NW Atlantic distal turbidites and their effects in the sedimentary record. Geology and Geochemistry of Abyssal Plains. Geological Special Publication, vol. 31, pp. 167–177.

Thomson, J., Jarvis, I., Green, D.R.H., Green, D.A., Clayton, T., 1998. Mobility and immobility of redox-sensitive elements in deep-sea turbidites during shallow burial. Geochim. Cosmochim. Acta 62 (4), 643–656.

UNEP/MAP/MED POL, 2003. Riverine transport of water, sediments and pollutants to the Mediterranean Sea. MAP Technical Reports Series, vol. 141. UNEP/MAP, Athens, Greece. 111 pp.

Vail, P.R., Mitchum Jr., R.M., Todd, R.G., Widmier, J.M., Thompson, S., Sangree, J.B., Bubb, J.N., Hatlelid, W.G., 1977. Seismic stratigraphy and global changes of sea level. In: Payton, C.E. (Ed.), Seismic Stratigraphy. Applications to Hydrocarbon Exploration. AAPG Mem., vol. 26, pp. 49–212.

Weedon, G.P., Shackleton, N.J., 1997. Inorganic geochemistry composition of Oligocene to Miocene sediments and productivity variations in the Western Equatorial Atlantic: results from sites 926 and 929. Proc. Ocean Drill. Program Sci. Results 154, 507–526.

Wehausen, R., Brumsack, H.-J., 1999. Cyclic variations in the chemical composition of eastern Mediterranean Pliocene sediments: a key for understanding sapropel formation. Mar. Geol. 153, 161–176.

Weldeab, S., Siebel, W., Wehausen, R., Emeis, K.-C., Schmiedl, G., Hemleben, C., 2003. Late Pleistocene sedimentation in the Western Mediterranean Sea: implications for productivity changes and climatic conditions in the catchment areas. Palaeogeogr. Palaeoclimatol. Palaeoecol. 2963, 1–17.

Zuo, Z., Eisma, D., Gieles, R., Beks, J., 1997. Accumulation rates and sediment deposition in the northwestern Mediterranean. Deep-Sea Res., Part 2, Top. Stud. Oceanogr. 44, 597–609.